

1    **The impact of organic nitrates on summer ozone formation in Shanghai,**  
2    **China**

3    Chunmeng Li<sup>1</sup>, Xiaorui Chen<sup>2, 3\*</sup>, Haichao Wang<sup>2, 3</sup>, Tianyu Zhai<sup>4</sup>, Xuefei Ma<sup>5</sup>, Xinping Yang<sup>4</sup>, Shiyi  
4    Chen<sup>5</sup>, Min Zhou<sup>6</sup>, Shengrong Lou<sup>6</sup>, Xin Li<sup>5</sup>, Limin Zeng<sup>5</sup>, Keding Lu<sup>5\*</sup>

5    <sup>1</sup> Center for Environmental Metrology, The National Institute of Metrology, Beijing 100029, China.

6    <sup>2</sup> School of Atmospheric Sciences, Sun Yat-sen University, Zhuhai, Guangdong, 519082, China.

7    <sup>3</sup> Guangdong Provincial Observation and Research Station for Climate Environment and Air Quality  
8    Change in the Pearl River Estuary, Key Laboratory of Tropical Atmosphere-Ocean System, Ministry  
9    of Education, Southern Marine Science and Engineering Guangdong Laboratory (Zhuhai), Zhuhai,  
10   519082, China.

11   <sup>4</sup> State Environmental Protection Key Laboratory of Vehicle Emission Control and Simulation,  
12   Chinese Research Academy of Environmental Sciences, Beijing, 100012, China

13   <sup>5</sup> State Key Joint Laboratory of Environmental Simulation and Pollution Control, The State  
14   Environmental Protection Key Laboratory of Atmospheric Ozone Pollution Control, College of  
15   Environmental Sciences and Engineering, Peking University, Beijing, 100871, China.

16   <sup>6</sup> State Environmental Protection Key Laboratory of the Cause and Prevention of Urban Air Pollution  
17   Complex, Shanghai Academy of Environmental Sciences, Shanghai, 200233, China.

18  
19   \* Correspondence: chenxr95@mail.sysu.edu.cn; k.lu@pku.edu.cn

20   **Abstract**

21   Organic nitrates serve as important secondary oxidation products in the atmosphere, playing a crucial  
22   role in the atmospheric radical cycles and influencing the production of secondary pollutants (ozone  
23   (O<sub>3</sub>) and secondary organic aerosols). However, field measurements of organic nitrates are scarce in  
24   China, and a comprehensive localized mechanism for organic nitrates is absent, hindering effective  
25   pollution mitigation strategies. In this study, we conducted measurements of ambient gaseous organic  
26   nitrates and examined their effects on local O<sub>3</sub> production at a polluted urban site in eastern China  
27   during summer. The average daytime concentrations of alkyl nitrates (ANs) and peroxy nitrates (PNs)  
28   throughout the campaign were 0.5±0.3 ppbv and 0.9±0.7 ppbv, respectively, with peaks reaching up to  
29   1.6 ppbv and 3.6 ppbv. An observation-constrained box model, incorporating an updated mechanism  
30   for organic nitrates, was employed to assess the environmental impact of these compounds. The model  
31   results indicated that PNs production inhibited the daytime O<sub>3</sub> production by 16% (0.8 ppbv/h), which  
32   is relatively low compared to previous studies. Furthermore, scenario analyses revealed that production  
33   yields ( $\alpha$ ) of ANs would alter the response of O<sub>3</sub> formation to precursors due to varying compositions  
34   of volatile organic compounds. Our results suggest that blind pollution control may cause ineffective  
35   pollution prevention and highlight the necessity of a thorough understanding on organic nitrate

36 chemistry for local O<sub>3</sub> control strategy.

37 **1. Introduction**

38 Tropospheric ozone, as an important oxidant, influences the atmospheric lifetimes of trace gases  
39 through its involvement in photochemical processes, thereby playing a crucial role in climate change  
40 and atmospheric chemistry. There is a broad consensus that high near-surface ozone concentrations are  
41 hazardous to human health and environmental ecosystems, particularly affecting the human respiratory  
42 and cardiovascular systems, and result in decreased yields of various crops (Ashmore, 2005; Xue and  
43 Zhang, 2023). A scientific assessment of tropospheric ozone is essential for the development of public  
44 health policies and for addressing long-term air pollution challenges (Monks et al., 2015). Primary  
45 pollutants, such as nitrogen oxides (NO<sub>x</sub>) and volatile organic compounds (VOCs), participate in the  
46 formation of HO<sub>x</sub> radicals (RO<sub>x</sub> = RO<sub>2</sub> + HO<sub>2</sub> + OH) cycles and NO<sub>x</sub> cycles under sunlight, leading to  
47 the continuous production of ozone as a secondary oxidation product within these cycles. In addition  
48 to the reaction between OH and NO<sub>2</sub> that produces HNO<sub>3</sub> as part of chain termination reactions, the  
49 interaction of RO<sub>2</sub> and NO that produces organic nitrates is of increasing concern (Present et al., 2020).  
50 The atmospheric production of organic nitrates consumes both NO<sub>x</sub> and RO<sub>2</sub>. Therefore, the chemistry  
51 of organic nitrates will significantly influence the prevention and control of ozone, with NO<sub>x</sub> and VOCs  
52 serving as independent variables.

53 Both anthropogenic activities and natural processes contribute to the emissions of NO<sub>x</sub> and VOCs,  
54 which produce RO<sub>2</sub> in the presence of oxidants such as OH. Subsequently, RO<sub>2</sub> reacts with NO to yield  
55 NO<sub>2</sub> and RO. After that, NO<sub>2</sub> photolysis produces O<sub>3</sub>, while RO is converted into HO<sub>2</sub> through an  
56 isomerization reaction, thereby forming the ozone production cycle. Within the cycle, a branching  
57 reaction between RO<sub>2</sub> and NO leads to the formation of alkyl nitrates (RONO<sub>2</sub>, ANs), while RO<sub>2</sub> may  
58 also react with NO<sub>2</sub> to generate peroxy nitrates (RO<sub>2</sub>NO<sub>2</sub>, PNs). Given that PNs are prone to thermal  
59 dissociation near the surface (Roberts and Bertman, 1992), they can influence O<sub>3</sub> production by  
60 modifying the availability of NO<sub>x</sub> and RO<sub>x</sub>. Due to the competitive production dynamics between PNs  
61 and O<sub>3</sub>, numerous field observations and model simulations have been conducted to investigate the  
62 impact of peroxyacetyl nitrate (PAN) on O<sub>3</sub> production (Liu et al., 2021; Zeng et al., 2019; Zhang et  
63 al., 2020). For ANs formation, the branching ratio ( $\alpha$ ), the reaction ratio  $k_{1b}/(k_{1a}+k_{1b})$ , varies between  
64 0.1-35%, which are associated with the carbon chain structure of the molecule, the distribution of  
65 functional groups, temperature, and pressure (Reisen et al., 2005; Arey et al., 2001; Wennberg et al.,  
66 2018; Russell and Allen, 2005; Butkovskaya et al., 2012; Cassanelli et al., 2007). Some values of  $\alpha$ ,  
67 which have not been quantified in the laboratory, are estimated through structure-activity relationships  
68 (Arey et al., 2001; Reisen et al., 2005; Teng et al., 2015; Yeh and Ziemann, 2014a; Yeh and Ziemann,  
69 2014b). Multiple field observations revealed a strong linear correlation between ANs and O<sub>3</sub>, with a  
70 correlation coefficient ( $r^2$ ) exceeding 0.5, further substantiating the competitive relationship between  
71 ANs and O<sub>3</sub> (Aruffo et al., 2014; Day et al., 2003; Flocke et al., 1998).



74 Currently, research on the effects of ANs on O<sub>3</sub> distribution is predominantly located in Europe  
75 and the United States. Following the first in situ measurement of total organic nitrates through thermal  
76 dissociation laser-induced fluorescence instrument (TD-LIF) by Day et al., field observations of total  
77 ANs have been continuously conducted to study the role of ANs in the nitrogen cycle (Aruffo et al.,

78 2014; Browne et al., 2013; Chen et al., 2017; Darer et al., 2011; Day et al., 2003; Sadanaga et al., 2016).  
79 In conjunction with field observations and model simulations, Farmer et al. were the first to indicate  
80 that ANs influence the sensitivity of  $\text{NO}_x$ -VOCs- $\text{O}_3$  (Farmer et al., 2011). As  $\text{NO}_x$  emissions decrease  
81 due to pollution control measures, ANs chemistry is expected to play an increasingly significant role  
82 in  $\text{O}_3$  simulations (Present et al., 2020; Zare et al., 2018). Current mechanisms for  $\text{O}_3$  simulations  
83 generally achieve reasonable predictions in large-scale models; however, they exhibit deviations  
84 exceeding 10 ppbv in regional simulations (Young et al., 2018). Subsequent studies have demonstrated  
85 that refining the ANs chemistry can further improve the simulation performance for  $\text{O}_3$  (Schwantes et  
86 al., 2020). ANs are predominantly produced through oxidation reactions facilitated by OH,  $\text{O}_3$ , and  
87  $\text{NO}_3$ . The daytime ANs are mainly contributed by the OH channel, whereas during nighttime, the  
88 contribution of the  $\text{NO}_3$  channel is linked to significantly increased yields of ANs (Liebmann et al.,  
89 2018; Ng et al., 2017; Zare et al., 2018). Presently, the enhancement of ANs chemistry mainly focuses  
90 on BVOCs, particularly isoprene and monoterpenes. These researches aim to enhance the yield of ANs  
91 derived from BVOCs, the re-release ratio of ANs to  $\text{NO}_x$ , and the contribution of ANs to aerosols  
92 (Fisher et al., 2016; Romer et al., 2016; Travis et al., 2016; Zare et al., 2018). Despite the establishment  
93 of a complete mechanism scheme at present, significant uncertainties remain in ANs simulation, which  
94 may introduce substantial uncertainties into the  $\text{O}_3$  simulation.

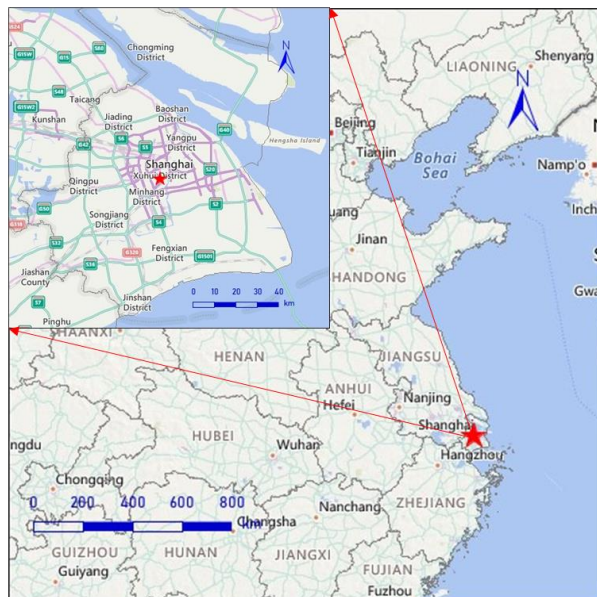
95 Atmospheric pollution is common across China, particularly in the Yangtze River Delta. Shanghai,  
96 as a highly urbanized metropolis in the Yangtze River Delta, has rendered the region's complex  
97 pollution due to its rapid economic growth and urbanization (Wang et al., 2022; Zhu et al., 2021).  
98 Previous studies have shown a significant increase in near-surface  $\text{O}_3$  levels from 2006 to 2016 in  
99 Shanghai (Gao et al., 2017). However, research on the ANs chemistry and their impact on  $\text{O}_3$  pollution  
100 remains limited in this area. In addition, most field measurements of ANs have focused on short-chain  
101 species (Ling et al., 2016; Song et al., 2018; Sun et al., 2018; Wang et al., 2013), which have been  
102 observed to exert a typical inhibition effect on daytime  $\text{O}_3$  production. A limited number of total ANs  
103 measurements found that both ANs and  $\text{O}_3$  production were in the VOC-limited regime (Li et al., 2023).  
104 To further investigate the influence of organic nitrates on  $\text{O}_3$  production, this study describes the  
105 distribution of organic nitrates based on a comprehensive field campaign conducted in Shanghai,  
106 analyzes the effects of organic nitrates on  $\text{O}_3$  production through model simulations, and offers  
107 recommendations for the prevention and control of ozone pollution in the region.

## 108 2. Methodology

### 109 2.1 Measurement site and instrumentations

110 A comprehensive campaign was conducted in Shanghai to further investigate the chemical  
111 behavior of organic nitrates in urban environments across China. As depicted in Fig. 1, the site is  
112 located in the Xuhui District of Shanghai (121.44°E, 31.18°N), in proximity to the Shanghai Inner  
113 Ring Viaduct, surrounded by numerous residential and office areas without significant industrial  
114 emission sources. The site is mainly influenced by morning-evening rush hours, as well as the transport  
115 of air masses to the urban location. The overall wind speed was low, predominantly originating from  
116 the east. All the measurement instruments were housed in the temperature-controlled room within the  
117 laboratory building at the Shanghai Academy of Environmental Sciences. Thermal Dissociation-

118 Cavity Enhanced Absorption Spectroscopy (TD-CEAS) was positioned on the 7th floor about 25 m  
119 above ground level, with the sampling tube extending out through the window.



120

121 **Figure 1.** Map of the city of Shanghai and the surrounding area (@ MeteoInfoMap). The red star is the location of  
122 the campaign site.

123 The Shanghai campaign focused on studying summer ozone pollution, with the chemical  
124 parameters presented in Table 1. Organic nitrates were measured by TD-CEAS with a sampling flow  
125 rate of 3 L/min and a sampling duration of 3 min for alternating measurements of NO<sub>2</sub>, PNs, and ANs.  
126 The sampling apparatus consisted of a 2-meter-long 1/4-inch tetrafluoroethylene (TFE) tube, through  
127 which the atmosphere was filtered through a TFE particulate filter. The membrane was replaced once  
128 a day to mitigate the interference caused by wall loss. The measurement of PAN was conducted by gas  
129 chromatography electron capture detection (GC-ECD). The Measurement of N<sub>2</sub>O<sub>5</sub> was performed via  
130 CEAS, which relies on the thermal dissociation of N<sub>2</sub>O<sub>5</sub> to yield NO<sub>3</sub>. Particulate nitrates and gaseous  
131 HNO<sub>3</sub> were measured online by AeRosols and GAses (MARGA), where soluble substances were  
132 quantified through ion chromatography following dissolution. The measurements of HONO were  
133 finished by CEAS during the campaign. Measurements of VOCs were achieved using a combination  
134 of GC-FID and GC-MS, with GC-MS predominating due to the limited species measured by GC-FID.  
135 The photolysis rate constant (J value) was determined using a spectrum radiometer with a time  
136 resolution of 20 s. Additionally, simultaneous measurements of other trace gases such as NO, NO<sub>2</sub>,  
137 SO<sub>2</sub>, CO, O<sub>3</sub>, and PM<sub>2.5</sub> were conducted using commercial instruments.

138 **Table 1.** Measured species for organic nitrates analysis and instrument time resolution, accuracy, and detection  
139 limitation.

Parameters	Measurement technique	Time resolution	Accuracy	Detection limit
ANs, PNs, NO <sub>2</sub>	TD-CEAS	3 min	± 8%	93 pptv
PAN	GC-ECD	5 min	± 10%	5 pptv
N <sub>2</sub> O <sub>5</sub>	CEAS	1 min	± 19%	2.7 pptv
NO	Thermo 42i	1 min	± 10%	60 pptv

NO <sub>2</sub>	Chemiluminescence	1 min	± 10%	300 pptv
HONO	CEAS	1 min	± 3%	100 pptv
Particulate nitrate	2060 MARGA	1 h	± 3%	0.01 $\mu\text{g}/\text{m}^3$
HNO <sub>3</sub>	2060 MARGA	1 h	± 3%	0.01 $\mu\text{g}/\text{m}^3$
SO <sub>2</sub>	Thermo 43i-TLE	1 min	± 16%	50 pptv
HCHO	Hantzsch fluorimetry	1 min	± 5%	25 pptv
CO	Thermo 48i-TLE	1 min	± 16%	50 pptv
O <sub>3</sub>	Thermo 49i	1 min	± 5%	0.5 ppbv
PM <sub>2.5</sub>	Thermo TEOM	1 min	± 5%	0.1 $\mu\text{g}/\text{m}^3$
VOCs	GC-FID/GC-MS	1 h	± 30%	20-300 pptv
J value	Spectrum radiometer	20 s	± 10%	$5 \times 10^{-5} \text{ s}^{-1}$

140

141

## 2.2 Model calculation

142 To investigate the impact of ANs chemistry on O<sub>3</sub> production, a box model was employed to  
 143 simulate the photochemistry processes. The mechanism of the model was enhanced based on RACM2  
 144 (Regional Atmospheric Chemical Mechanism version 2). This box model simulates the  
 145 physicochemical processes occurring within a defined volume for each reactant. It utilizes measured  
 146 parameters as the boundary condition to simulate the chemistry process while allowing for convenient  
 147 adjustments to the mechanism. The model generates files detailing concentration changes, budget  
 148 processes, and reaction rates, thereby providing an efficient means to simulate ground-level pollutants.  
 149 In this study, the box model was constrained by various parameters, including J values, O<sub>3</sub>, NO, NO<sub>2</sub>,  
 150 CO, HONO, VOCs, RH, temperature, and pressure, with the time step set to 1h. The deposition process  
 151 was quantified using the deposition rate and the boundary layer height, with the dry deposition rate  
 152 established at 1.2 cm/s and the boundary layer height constrained by data obtained from NASA.

153 The RACM2 facilitates classification through the distribution of functional groups and  
 154 subsequently delineates reactions involving 17 stable non-organic compounds, 4 inorganic  
 155 intermediates, 55 stable organic compounds, and 43 intermediate organic species within the  
 156 mechanism. However, the mechanism description for ANs is notably abbreviated. The various ANs,  
 157 characterized by differing functional groups, are treated as a unified entity, thereby neglecting the  
 158 influence of functional groups on the underlying chemistry. Consequently, this study builds on the  
 159 previous research and further evaluates the updates of the mechanism (Li et al., 2023). These  
 160 mechanistic updates are developed based on the work of Zare et al. and primarily encompasses the  
 161 oxidation processes of BVOCs by OH and NO<sub>3</sub>, as well as the deposition and the aerosol uptake, which  
 162 are detailed in the SI (Zare et al., 2018). Accordingly, three mechanistic schemas are compared based  
 163 on the campaign, which will be elaborated upon in subsequent sections. A box model based on the  
 164 above mechanism is used to calculate the ozone production rate (P(O<sub>3</sub>)) (Tan et al., 2017b). P(O<sub>3</sub>) was  
 165 quantified based on the net production rate of O<sub>x</sub> (the sum of O<sub>3</sub> and NO<sub>2</sub>), by subtracting the O<sub>x</sub>  
 166 depletion from the instantaneous O<sub>x</sub> production. The simulation uncertainty of the box model is about  
 167 40%, introduced mainly by the simplified reaction rate constants, photolysis rate constants, and near-  
 168 ground deposition (Lu et al., 2013). The impact of PNs photochemistry on local ozone is quantified by  
 169 comparing the difference of the daytime P(O<sub>3</sub>) between the scenarios with and without PNs

photochemistry via a chemical box model. Here, the PNs photochemistry includes the production and removal of PAN, MPAN and PPN.

To facilitate the assessment of the impacts of ANs on local  $O_3$  pollution, we further conducted a simplified box model based on the steady-state assumption approach. Several studies have examined the combined effect of  $\alpha$  and VOCs reactivity on local  $O_3$  levels using this approach (Farmer et al., 2011; Present et al., 2020; Romer et al., 2016; Romer et al., 2018). Briefly, the production pathway of ANs is simplified according to VOCs categories and the production rate of OH and  $HO_2$  ( $P(HO_x)$ ) is fixed to a constant value. VOCs are categorized into two primary groups: non-oxygenated VOCs (RVOCs) and oxygenated VOCs (OVOCs). Both categories of VOCs undergo oxidation by OH, resulting in the formation of  $RO_2$ , specifically  $RVOCRO_2$  and  $OVOCRO_2$ . The interaction between  $RVOCRO_2$  and NO will produce  $\alpha$  ANs,  $(1-\alpha) NO_2$ ,  $HO_2$ , and OVOC. Conversely, the reaction of  $OVOCRO_2$  with NO directly generates  $NO_2$ . In the Beijing-Tianjin-Hebei, Yangtze River Delta, and Chengdu-Chongqing regions of China,  $P(HO_x)$  is approximately 4 ppbv/h (Lu et al., 2013; Tan et al., 2018a; Tan et al., 2018b).  $P(HO_x)$  is therefore assumed to be 4 ppbv/h, with equal production rates of OH and  $HO_2$ . The model also incorporates additional processes, including inter- and self-reactions of  $RO_2$ , as well as reactions between  $NO_2$  and NO, and deposition processes. In addition, during the daytime, NO is determined by  $j(NO_2)$ ,  $O_3$ , and  $NO_2$  according to the photo-stationary state among  $NO$ - $NO_2$ - $O_3$ . Based on the above simplified approach, production rates of ANs and  $O_3$  in this study can be derived by direct calculations.

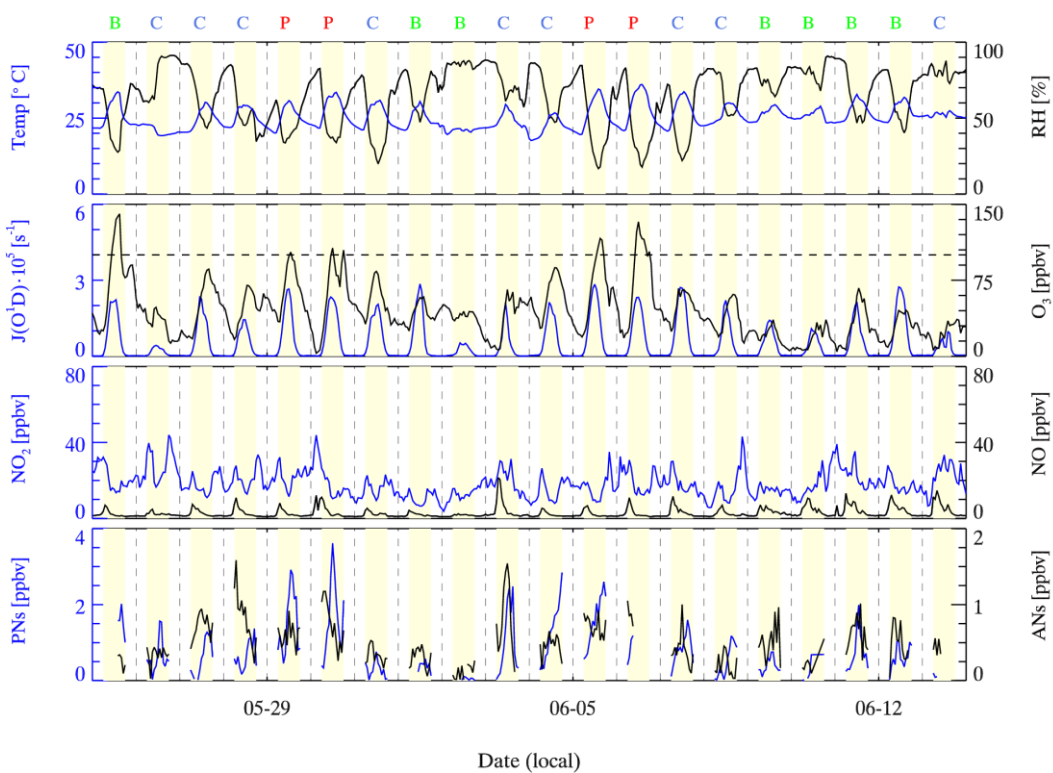
To investigate the effects of  $NO_x$  and VOCs on  $O_3$  production, the theoretical maximum of  $P(O_3)$  was simulated by a box model under varying concentrations of  $NO_x$  and VOCs. This approach was employed to develop an empirical kinetic modeling approach for ozone production (EKMA). The EKMA serves as a model sensitivity method to inform strategies for pollutant abatement. In this study, EKMA utilizes the measured mean parameters as the initial point. Each parameter was incrementally adjusted in 30 equidistant steps to create scaled arrays of VOCs and  $NO_x$ , which were subsequently used to simulate the variations in  $P(O_3)$  resulting from changes in precursor concentrations. Ultimately, contour plots illustrating the relationship between  $P(O_3)$  arrays versus the concentrations of  $NO_x$  and VOCs are plotted based on the simulation results.

### 3. Results and discussions

#### 3.1 Overview of organic nitrates and precursors

The duration of the Shanghai campaign was 20 days, spanning from May 25 to June 13, 2021. The analysis of organic nitrates is performed from 6 a.m. to 6 p.m., as measurements taken during nighttime were subject to interference from  $N_2O_5$  and its derivatives, a phenomenon noted in previous studies (Li et al., 2021; Li et al., 2023). Simultaneous measurements of PAN and PNs were conducted throughout the campaign. There was a malfunction of the GC-ECD instrument from June 12 to June 13, during which the measurements of PAN were generally low. Relative humidity (RH) varied considerably, with over 95% during rainfall periods on June 2, June 9, June 10, and June 13, while the remaining days were predominantly sunny. Temperatures were high, with minimums of 20 °C and daytime peaks reaching up to 36 °C. The wind speeds were generally high during the daytime and low at night, with maximum of 4.2 m/s. The easterly winds prevailed during the campaign, except for May

210 27-28 and June 3-6 with mostly west and southwest winds.



211

212 **Figure 2.** The time series of the related parameters focused on organic nitrates during the campaign. The background  
213 days are represented by green B, the clean days are represented by blue C, and the ozone pollution day is represented  
214 by red P.

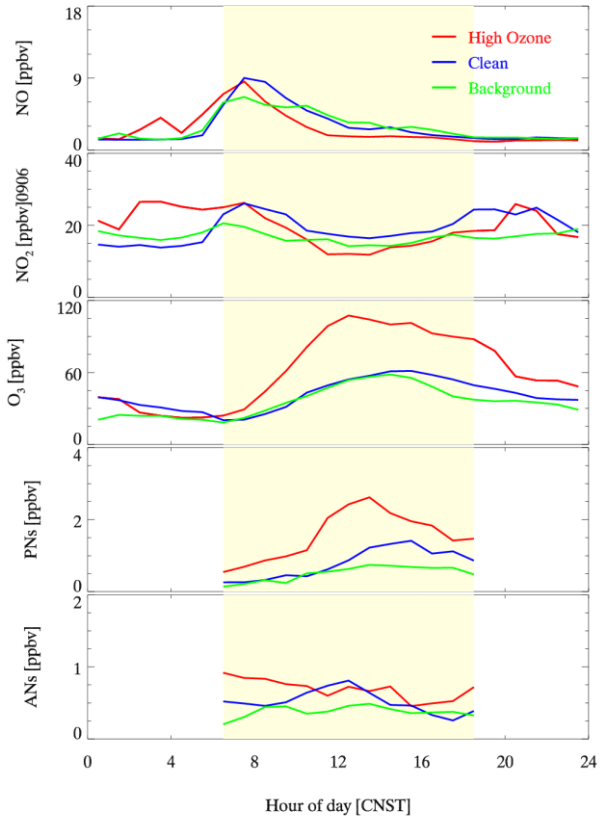
215 According to Chinese air quality standards for Class II areas, which define ozone pollution days  
216 as those with an hourly average exceeding 100 ppbv, the periods from May 29 to May 30 and June 5  
217 to June 6 have been identified as ozone pollution days. The days without ozone pollution are  
218 categorized as clean or background days. For clean days, parameters, including  $\text{KOH}$ ,  $\text{SO}_2$ , and  $\text{CO}$ ,  
219 show significant diurnal variations (Fig S1), and no rain occurs. The days that are neither ozone  
220 pollution days nor clean days are then classified as background days. The daytime averages of  
221 environmental parameters during the ozone pollution period, the clean period, and the background  
222 period are presented in Table 2. Excluding cloudy and rainy days, the daytime peak of  $\text{J}(\text{O}^1\text{D})$  was  
223 near  $2.8 \times 10^5 \text{ s}^{-1}$ , indicating a high photochemical oxidation potential. As a secondary photochemical  
224 product,  $\text{O}_3$  exhibited a typical daily profile, peaking at 140.5 ppbv throughout the campaign. The  
225 measurements of PNs peaked at 3.6 ppbv with a daytime average of  $0.5 \pm 0.3$  ppbv, while ANs peaked  
226 at 1.6 ppbv with a daytime average of  $0.5 \pm 0.3$  ppbv. Ozone pollution periods were often associated  
227 with high organic nitrates. The mean daily variation of  $\text{NO}_x$  was consistent with the characteristics of  
228 typical urban sites, significantly influenced by the morning-evening rush hours. During the daytime,  
229 NO exhibited a single peak distribution, whereas  $\text{NO}_2$  displayed a bimodal distribution. In comparison  
230 to the background and clean period, the ozone pollution period was characterized with higher  
231 temperatures and lower humidity. Additionally, the photolysis rate and levels of  $\text{PM}_{2.5}$  were both  
232 elevated during pollution days.

233 **Table 2.** Summary of daytime averages of chemical parameters over different periods during the Shanghai campaign.

Phase	Ozone pollution	Background	Clean
T/°C	29.8±3.7	27.0±3.4	26.0±3.5
P/hPa	1043.6±0.8	1045.3±0.9	1044.3±1.4
RH/%	39.2±13.9	65.2±16.0	62.4±17.2
J(O <sup>1</sup> D)×10 <sup>5</sup> /s	1.3±0.9	0.9±0.8	0.8±0.8
J(NO <sub>2</sub> )×10 <sup>3</sup> /s	4.5±2.1	2.8±2.0	2.6±1.9
NO <sub>2</sub> /ppbv	17.3±6.1	16.5±5.8	20.3±7.4
NO/ppbv	3.2±2.6	4.0±2.7	4.2±3.7
O <sub>3</sub> /ppbv	78.6±30.9	41.6±27.7	45.0±21.5
PM <sub>2.5</sub> /μg·m <sup>-3</sup>	25.9±4.3	18.3±13.4	21.9±10.0
SO <sub>2</sub> /ppbv	2.2±1.7	0.4±0.5	0.6±0.7
CO/ppbv	505.3±64.3	441.6±133.3	535.0±147.8
ISO/ppbv	0.1±0.1	0.2±0.2	0.1±0.1

234

235 The mean diurnal profiles of organic nitrates and related parameters observed during the campaign  
 236 are shown in Fig. 3. During the ozone pollution period, NO<sub>x</sub> exhibited a peak concentration at 3:00  
 237 a.m., especially NO, which indicates a contribution from local emission at this site. In comparison to  
 238 the clean period, daytime NO<sub>x</sub> was lower during the ozone pollution period, particularly at noon when  
 239 NO dropped to as low as 1.7 ppbv. Correspondingly, ANs during the ozone pollution period were  
 240 generally high, but the daily variation was not significant. Therefore, the sources of ANs were more  
 241 complex during the ozone pollution period, involving both transport contribution and local production,  
 242 which aligns with the significantly increased background O<sub>3</sub>. During the clean period, the daytime  
 243 peak of O<sub>3</sub> was notably reduced and occurred later in the day. The fluctuations in NO<sub>x</sub> were more  
 244 closely associated with morning and evening rush hours. The daytime peak of PNs decreased from 2.6  
 245 ppbv to 1.4 ppbv. In addition, the diurnal profile of ANs displayed a more pronounced peak at noon.  
 246 During the background period, there was a further decline in the daytime peaks of NO<sub>x</sub> compared to  
 247 the clean period. The diurnal profile of O<sub>3</sub> exhibited similar trends, but the duration of high O<sub>3</sub> was  
 248 significantly shortened. The levels of both PN<sub>s</sub> and ANs exhibited a decline, approaching the  
 249 background concentrations.



250

251 **Figure 3.** Mean diurnal profiles of organic nitrates and related parameters during different observation periods.

252 Here, we compare our observations with the study previously conducted in Xinjin, which is a  
 253 suburban site, located in basin topography and faces emerging ozone pollution recently, to determine  
 254 the effect of organic nitrate on  $O_3$  production under different pollution conditions (Li et al., 2023). The  
 255 Shanghai and Xinjin campaigns were conducted in early and late summer, respectively, exhibiting  
 256 similar meteorological conditions. Photochemical conditions during both two campaigns are  
 257 comparable, with the daily means of  $J(O^1D)$  were  $0.9 \times 10^{-5} \text{ s}^{-1}$  and  $0.8 \times 10^{-5} \text{ s}^{-1}$ , while the daily means  
 258 of  $J(NO_2)$  were  $3.1 \times 10^{-3} \text{ s}^{-1}$  and  $3.0 \times 10^{-3} \text{ s}^{-1}$ , respectively, during Shanghai and Xinjin campaigns.  
 259 The ratio of NO to  $NO_2$  was 0.19 and 0.17 at Shanghai and Xinjin, respectively. Meanwhile, the  
 260 concentration of  $NO_x$  observed in Shanghai site (daily averages of 22.0 ppbv) is higher than that  
 261 observed in Xinjin site (daily averages of 12.5 ppbv). The concentrations of  $SO_2$  and CO at Shanghai  
 262 site were 0.9 and 491.4 ppbv, while  $SO_2$  and CO were 0.6 and 404.5 ppbv, respectively. Therefore, the  
 263 air masses at Shanghai site were less aged than Xinjin site. However, the concentration of VOCs is  
 264 lower in Shanghai campaign compared to Xinjin campaign, with daily mean of 23.5 ppbv compared  
 265 to 22.4 ppbv. Therefore, a comparison of the two campaigns facilitates a comprehensive analysis of  
 266 the impacts of organic nitrate chemistry on local ozone pollution.

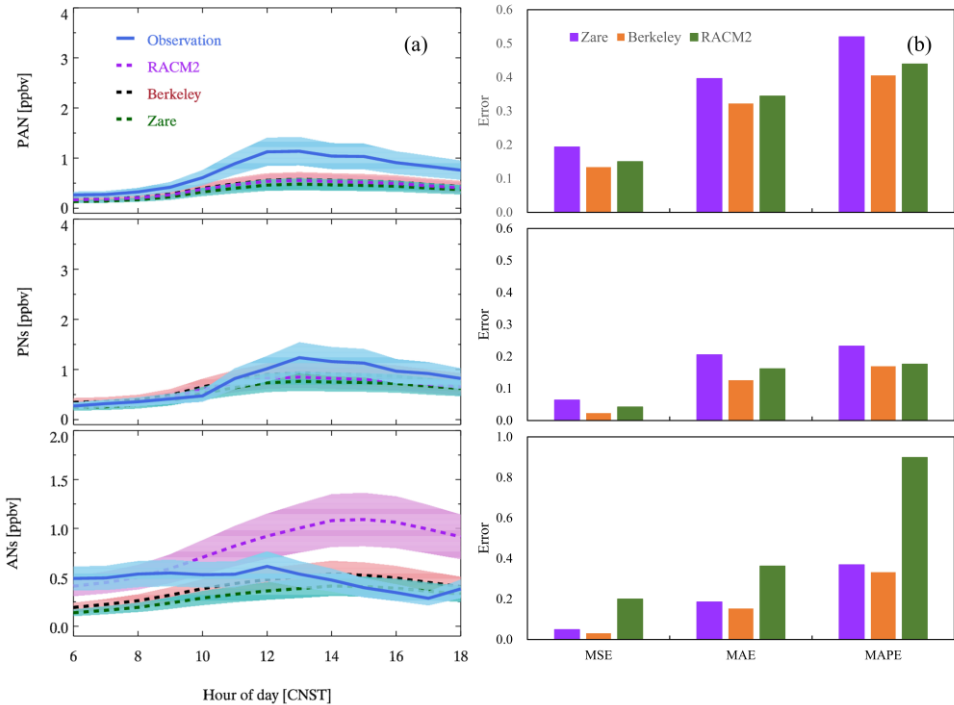
267 **3.2 Evaluation of organic nitrates simulations**

268 In light of the updates to the mechanisms, validation testing has been conducted. Our previous  
 269 study of the Xinjin campaign evaluated three mechanism schemes: mechanism S0, which is based on  
 270 RACM2, mechanism S1 and mechanism S2 which refines the budget for BVOC-derived organic

271 nitrates (Li et al., 2023). It was found that the performance of mechanism S2 for organic nitrates  
272 exhibited an improvement exceeding 50%. Mechanism S2 has been updated by the Berkeley group  
273 (Fisher et al., 2016; Travis et al., 2016), which includes enhancements to the production mechanism of  
274 isoprene, the incorporation of the production mechanism for monoterpenes, and the completion of the  
275 uptake of organic nitrates by aerosols. Additionally, the Zare mechanism further refines the production  
276 mechanism of organic nitrates initiated by OH and  $\text{NO}_3$ , as well as improving the deposition process  
277 of organic nitrates. As a result, the Shanghai campaign was simulated using RACM2, Berkeley, and  
278 Zare mechanisms respectively for comparison.

279 The simulation result of organic nitrates under the three mechanisms is shown in Fig. 4a. The  
280 simulations for PAN or PNs exhibit an overall underestimation tendency, with the simulation of PAN  
281 demonstrating an even greater underestimation. Notably, the measured PNs remained above 500 pptv  
282 during nighttime, indicating a continuous transportation contribution at this site. Furthermore, the  
283 underestimation of PNs may be attributed to the unidentified  $\text{RO}_x$  sources. It is consistent with the  
284 findings from summer campaigns in Wangdu, Beijing, where an underestimation of  $\text{RO}_2$  was noted,  
285 particularly pronounced at elevated ambient  $\text{NO}_x$  (Tan et al., 2017a). In terms of ANs, the simulation  
286 performances vary across different mechanisms. A significant overestimation of ANs is evident when  
287 utilized RACM2. Conversely, the simulation based on the Berkeley and Zare mechanisms generally  
288 results in an underestimation of ANs, while the underestimation of the Zare mechanism is more  
289 significant. Sensitivity tests conducted in Xinjin campaign suggested that the simple representation of  
290 ANs uptake caused the underestimation (Li et al., 2023), which is the same reason of underestimation  
291 in the Shanghai campaign. The uptake of ANs need further experimental data to achieve a detailed  
292 description to support the simulations.

293 The diurnal profile of simulated PNs is consistent with the measurements, both reaching their  
294 daytime peak shortly after sunrise. However, it is noteworthy that the peak concentration of PNs  
295 measurements is significantly higher than the simulation. In a similar pattern with PNs, the simulated  
296 ANs began to accumulate around 6:00 a.m. The measured ANs reached their peak near noon, whereas  
297 the simulations peaked at 3:00 pm. To evaluate the performance of simulations, as showed in Fig. 4b,  
298 three types of error ratios were calculated: Mean Square Error (MSE), Mean Absolute Error (MAE),  
299 and Mean Absolute Percentage Error (MAPE). Different error metrics for the organic nitrates exhibit  
300 a similar trend. The simulation performances of the Berkeley mechanism are better than the other two  
301 mechanisms. It should be noted that the Berkeley mechanism failed to fully reproduce the diurnal  
302 pattern of observed ANs. This is mainly due to the atmospheric transport that contributes to the ANs  
303 as mentioned in section 3.1. In addition, the drastic changes in  $\text{NO}_x$  during rush hours will introduce  
304 errors to the ANs measurements. In addition, the Zare mechanism refined the oxidation of BVOCs by  
305 OH or  $\text{NO}_3$  by introducing extra species with uncertain yields, which might bring biases to the  
306 simulations under high  $\text{NO}_x$  and anthropogenic VOCs. In general, the Berkeley mechanism performs  
307 better on simulation of ANs than Zare mechanism. As a result, the subsequent analysis is based on the  
308 Berkeley mechanism.

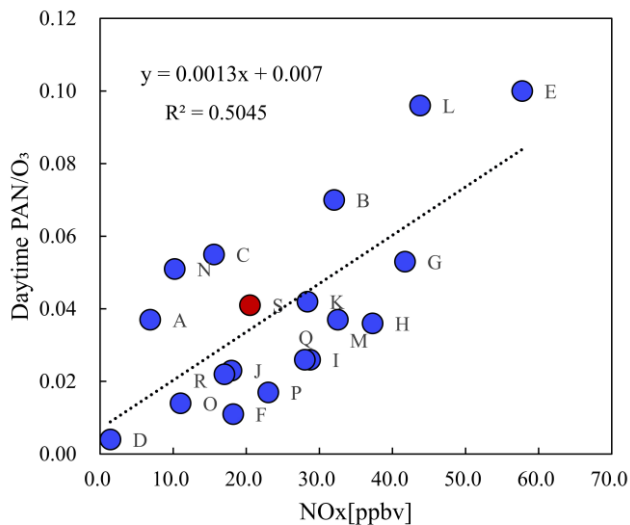


309

310 **Figure 4.** Mean diurnal profiles of observed and simulated ANs and PN<sub>s</sub> under different mechanism constraints  
 311 during the Shanghai campaign (a), and the error of the different cases (b), including mean square error (MSE), mean  
 312 absolute error (MAE) and mean absolute percentage error (MAPE).

313 **3.3 Impact of PN<sub>s</sub> chemistry on local ozone production**

314 Organic nitrates and O<sub>3</sub> have common precursors, and therefore the atmospheric behavior of  
 315 organic nitrates has an important influence on the local O<sub>3</sub> distribution. The production of PN<sub>s</sub>  
 316 consumes NO<sub>2</sub> and RO<sub>x</sub>, thereby directly impacting O<sub>3</sub> production. The relationship between the  
 317 distribution of PN<sub>s</sub> and O<sub>3</sub> is examined throughout the campaign. The observed PAN, PN<sub>s</sub> and O<sub>3</sub>  
 318 between 9:00 a.m. and 2:00 p.m. are selected for the analysis to mitigate interference from sources that  
 319 are not produced during daytime. The correlation of PAN or PN<sub>s</sub> with O<sub>3</sub> are shown in Fig. S2. Both  
 320 PAN and PN<sub>s</sub> demonstrate a strong correlation with O<sub>3</sub> with the ratio of PAN or PN<sub>s</sub> to O<sub>3</sub> being 0.041  
 321 or 0.058. High ratios of PN<sub>s</sub> and O<sub>3</sub> usually indicate severe pollution episodes (Shepson et al., 1992;  
 322 Sun et al., 2020; Zhang et al., 2023; Zhang et al., 2014). The minimum ratio of PN<sub>s</sub> to O<sub>3</sub> (0.024) was  
 323 found during the clean periods, which can be regarded as the threshold for local photochemical  
 324 pollution. NO<sub>x</sub> is the key pollutant for production of O<sub>3</sub> and PN<sub>s</sub>, in order to study the relationship  
 325 between the ratio of PAN or PN<sub>s</sub> to O<sub>3</sub> and NO<sub>x</sub>. The daytime ratios of PAN to O<sub>3</sub> derived from  
 326 historical field observations are summarized with corresponding NO<sub>x</sub> concentrations in Fig. 5. The  
 327 ratio derived from this study was distributed in the medium level of historical observations. The linear  
 328 correlation of NO<sub>x</sub> and the ratio of PAN to O<sub>3</sub> ratio suggests that the NO<sub>x</sub> concentration controls the  
 329 relative production of PN<sub>s</sub> and O<sub>3</sub>.



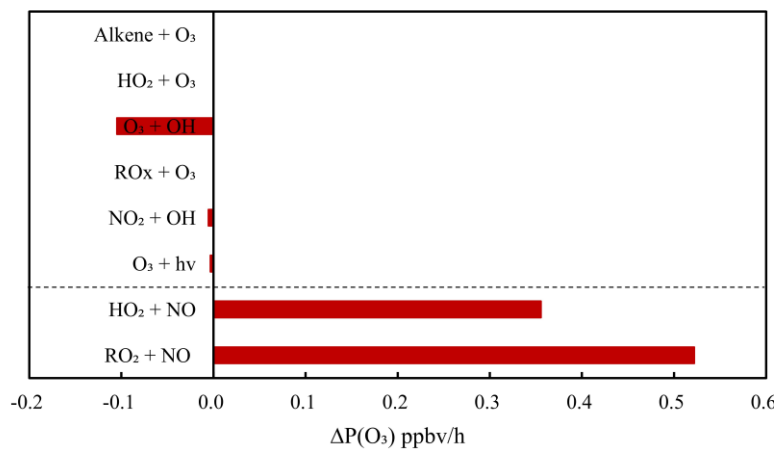
330

331 **Figure 5.** The relationship between historical daytime ratio of PAN to O<sub>3</sub> and NO<sub>x</sub> concentrations. The red dot is the  
 332 Shanghai campaign, and the blue dots are the historical campaigns. A: Grosjean et al., 2002 (Grosjean et al., 2002);  
 333 B: Lee et al., 2008 (Lee et al., 2008), C: Zhang et al., 2014 (Zhang et al., 2014), D-E: Zhang et al., 2009 (Zhang et  
 334 al., 2009), F-G: Zeng et al., 2019 (Zeng et al., 2019), H-K: Zhang et al., 2019 (Zhang et al., 2019), L-M: Sun et al.,  
 335 2020 (Sun et al., 2020); N: Li et al., 2023 (Li et al., 2023), O-R: Xu et al., 2024 (Xu et al., 2024), S: this study.

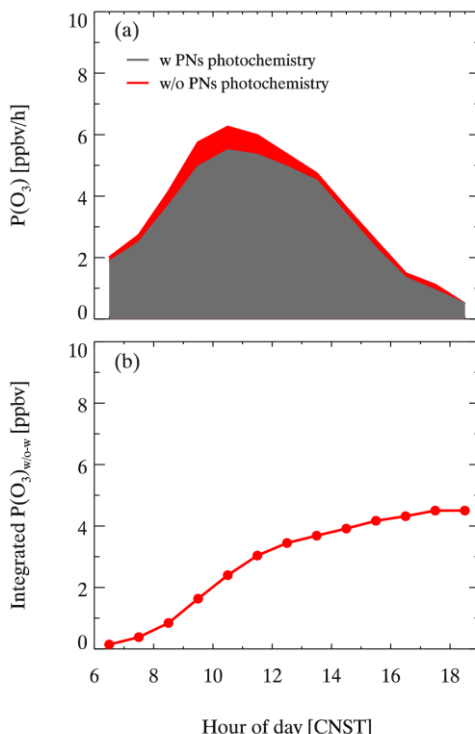
336 Sensitivity tests were conducted based on the box model to quantify the impact of PN  
 337 photochemistry on O<sub>3</sub> budgets. The differences of each pathway rate are calculated at the peak of O<sub>3</sub>  
 338 production rate (Fig. 6). In the absence of PN photochemistry, two primary source pathways -namely, the  
 339 reaction between RO<sub>2</sub> and NO, and the reaction between HO<sub>2</sub> and NO-exhibit large enhancements of  
 340 0.52 and 0.36 ppbv/h, respectively. In comparison, O<sub>3</sub> sinks increase slightly in the absence of PN  
 341 photochemistry, with the reaction between OH and O<sub>3</sub> showing the most significant enhancement of  
 342 0.11 ppbv/h. Therefore, during the Shanghai campaign, PN photochemistry suppressed daytime ozone  
 343 production mainly by reducing the reaction between HO<sub>2</sub> or RO<sub>2</sub> and NO.

344

345 **Figure 6.** The simulated difference of ozone produce rate ( $\Delta P(O_3)$ ) at 11am between the constraint of the PN  
 346 photochemistry and without the PN photochemistry.



347 The PNs maintain a notable concentration until 6:00 p.m., suggesting a persistent impact on local  
 348 ozone production. As shown in Fig. 7a, the PNs photochemistry began to inhibit ozone production as  
 349 early as 6 a.m. and increased up to 0.8 ppbv/h (16%) at 10 a.m. The integrated inhibition of PNs  
 350 photochemistry on  $O_3$  production was 4.5 ppbv in the Shanghai campaign (Fig. 7b), which was less  
 351 pronounced than the Xinjin campaign (20 ppbv). The reduced inhibition can be attributed to the lower  
 352 PNs production rate ( $P(PNs)$ ) observed in the Shanghai campaign (Fig. S3), where the maximum  
 353 daytime  $P(PNs)$  was 0.89 ppbv/h, much lower than that in Xinjin campaign (3.09 ppbv/h). In addition,  
 354 the two campaigns had similar concentrations of VOCs, but daytime average of  $NO_x$  in Shanghai site  
 355 is 22.0 ppbv, which is much higher than that of Xinjin site (10.2 ppbv). The PNs formation would be  
 356 reduced under high  $NO_x$  condition due to the rapid termination reaction via OH and  $NO_2$ , and thus  
 357 limited the suppression effect of PNs formation which is the case in Shanghai campaign. Like in Xinjin  
 358 campaign, PAN chemistry suppressed  $O_3$  formation at a rate of 2.84 ppbv/h at a suburban site in Hong  
 359 Kong (Zeng et al., 2019). However, it was reported that PAN tended to suppress  $O_3$  production under  
 360 low- $NO_x$  and low- $RO_x$  conditions but enhanced  $O_3$  production with sufficient  $NO_x$  at a rural coastal  
 361 site in Qingdao, which is consistent with the comparison of Xinjin and Shanghai campaigns (Liu et al.,  
 362 2021). The impacts of PNs photochemistry on  $O_3$  vary across different days. As shown in Fig. S4, the  
 363 integrated  $P(O_3)$  change reaches 6.9 ppbv due to PNs photochemistry during ozone pollution period.  
 364 For the background and clean periods, the changes are close to each other with a value of 3.8 and 4.2  
 365 ppbv, respectively. Therefore, the PNs photochemistry contributes to more  $P(O_3)$  inhibition during the  
 366 ozone pollution period, which should be considered in ozone pollution prevention.

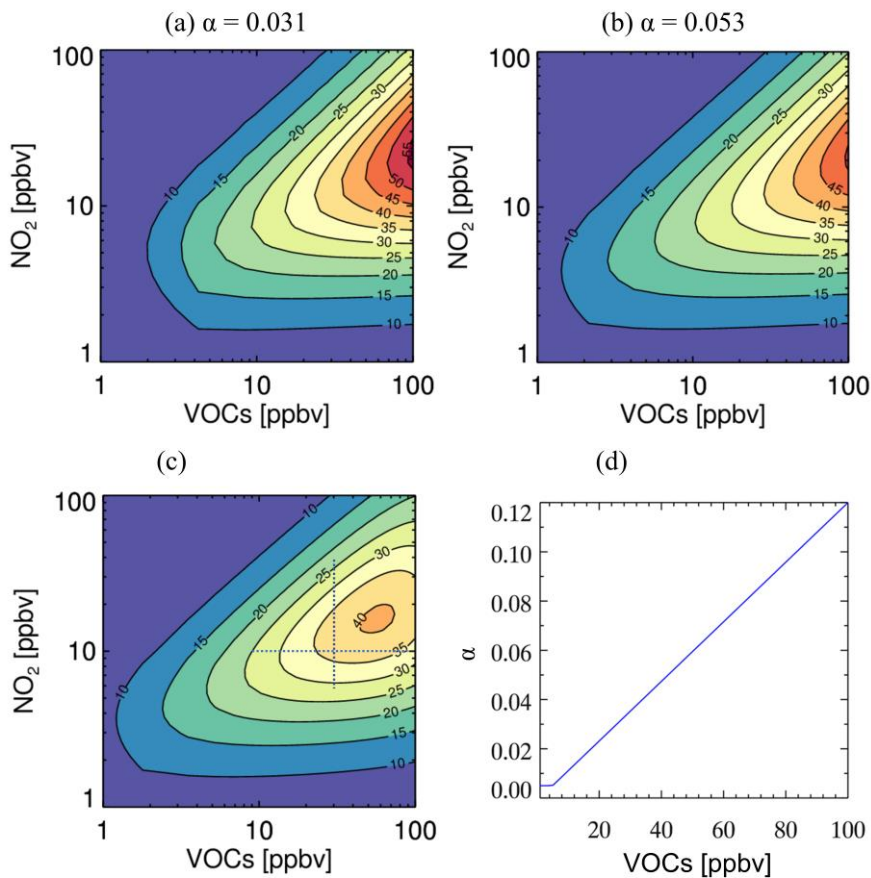


367

368 **Figure 7.** The impact of PNs photochemistry on  $P(O_3)$  during the Shanghai campaign (a) daily changes of  $P(O_3)$   
 369 under the constraint of PNs photochemistry, (b) integrated  $P(O_3)$  change constrained by PNs photochemistry.

370 **3.4 Impact of ANs chemistry on local ozone production**

371 To elucidate the impact of the  $\alpha$  on  $O_3$  production, the EKMA was utilized to investigate the  
 372 combined response of  $NO_x$  and VOCs to  $O_3$  production at different  $\alpha$ . The  $O_3$  production was calculated  
 373 by a simplified approach in method 2.2 and the  $\alpha$  values were derived from weighted average of  $\alpha$   
 374 based on the measured VOCs, the corresponding OH reaction rate constant and the  $\alpha$  (Table S1) in  
 375 Shanghai and Xinjin campaign, respectively. The model is initiated by the daytime averages of the  
 376 environmental parameters. A comparative analysis is conducted between the Xinjin campaign and the  
 377 Shanghai campaign where effective  $\alpha$  is determined to be 0.031 and 0.053, respectively. As illustrated  
 378 in Fig. 8a&b,  $P(O_3)$  exhibits a similar trend with the variations of  $NO_x$  and VOCs under different  $\alpha$ ,  
 379 while the value of  $P(O_3)$  reduces with larger  $\alpha$  at the same levels of precursors. For example, when  
 380 VOCs is at 8 ppbv and  $NO_x$  reaches 9 ppbv, the  $P(O_3)$  is 30.4 ppbv/h with  $\alpha$  of 0.031, whereas it  
 381 decreases to 24.6 ppbv/h when  $\alpha$  is 0.053. In addition, the larger of  $\alpha$  in the Shanghai campaign  
 382 increases the threshold of  $NO_x$  concentration for the transition of  $O_3$  production regime. When the  
 383 concentration of VOCs is fixed, a higher effective  $\alpha$  results in a lower  $NO_x$  concentration corresponding  
 384 to the peak of  $P(O_3)$ . Consequently, an increase in  $\alpha$  suppresses the peak of  $P(O_3)$  and simultaneously  
 385 affects its sensitivity to  $NO_x$  and VOCs concentrations.



386

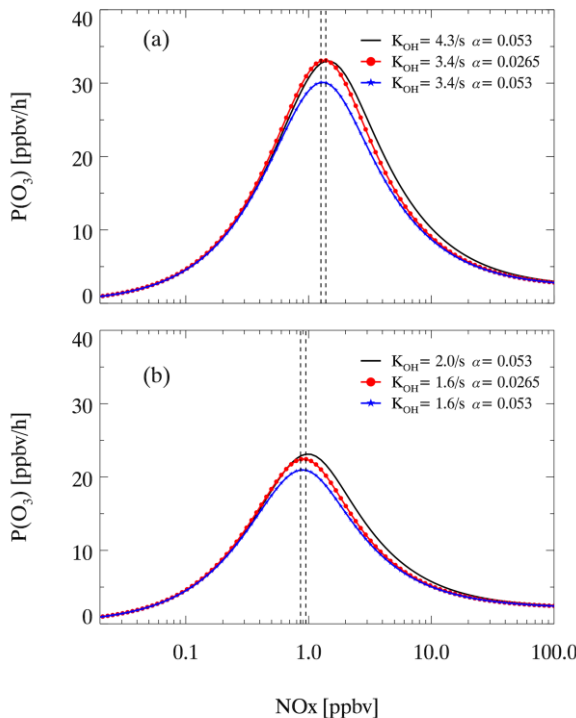
387 **Figure 8.** Ozone production ( $P(O_3)$ , ppb h<sup>-1</sup>) derived from a simplified analytic model is plotted as a function of  $NO_x$   
 388 and VOCs under three different organic nitrate scenarios with branching ratios of (a) 0.031 for the Xinjin campaign,  
 389 (b) 0.053 for the Shanghai campaign, and (c)VOC-dependent branching ratios for Shanghai campaign, where the

390 branching ratio decreases linearly from 12 to 0.5% with VOCs from 100 to 5 ppbv as shown in (d).

391 In the real atmosphere, the effective  $\alpha$  of ANs tends to exhibit a decline with the reduction of  
392 VOCs concentration. Historical studies show the general range from 0.03 to 0.04 in rural sites and  
393 from 0.04 to 0.10 in urban environments, depending on the composition of VOCs and the  $\alpha$  for BVOCs  
394 (Farmer et al., 2011; Perring et al., 2010; Perring et al., 2013; Perring et al., 2009; Rosen et al., 2004b).  
395 For simplicity, we use a linear relationship between  $\alpha$  and VOC concentration in the sensitivity analysis,  
396 as shown in Fig. 8d. An  $\alpha$  value of 0.005 was selected for clean condition with VOC concentration less  
397 than 5 ppbv, while 0.12 was selected for polluted condition with VOC concentration larger than 100  
398 ppbv. The lower limit of 0.005 is the average of the  $\alpha$  for methane and ethylene. The upper limit of  
399 0.12 is set as the reported value of the  $\alpha$  for isoprene and the  $\alpha$  for aromatic hydrocarbons are generally  
400 distributed around 0.1 (Perring et al., 2013). The assumption of this linear relationship between  $\alpha$  and  
401 VOC concentration has also been applied in a previous study (Farmer et al., 2011). With a varying  $\alpha$ ,  
402 as shown in Fig. 8d,  $P(O_3)$  does not follow a consistent downward trend as VOCs decrease in VOC-  
403 limited regime or transition regime. Instead, with the decrease of VOCs, the  $P(O_3)$  is likely to increase  
404 at first at a relatively high VOCs distribution, and then decrease similar to the fixed  $\alpha$  scenario. Take  
405 the cases of the horizontal dashed line as an example, at a fixed  $NO_x$ , the  $P(O_3)$  increases as the VOCs  
406 decrease within the range of about 60 to 100 ppbv, whereas  $P(O_3)$  subsequently decrease as VOCs fell  
407 below 60 ppbv. Therefore, with the reduction in VOCs emission, an increase in  $\alpha$  directly correlates  
408 with a reduction in the  $P(O_3)$  peak. As a result, a positive correlation between  $\alpha$  and VOCs  
409 concentrations in real atmosphere might alter the  $NO_x$ -VOCs- $O_3$  relationship and diminish the effects  
410 of VOCs reduction on ozone control.

411 Scenarios with different VOCs reactivity and  $\alpha$  are selected for sensitivity tests to further  
412 investigate the impact of ANs chemistry on the  $O_3$  pollution control strategy in Shanghai. As illustrated  
413 in Fig. 9a, variations of  $P(O_3)$  among three scenarios exhibit an initial increase followed by a  
414 subsequent decrease with rising  $NO_x$ . For the typical VOC reactivity and  $\alpha$  obtained from the Shanghai  
415 campaign, the turning point from  $NO_x$  benefit to  $NO_x$  limitation for  $P(O_3)$  occurs at  $NO_x$  concentration  
416 of 1.38 ppbv, when  $P(O_3)$  reaches a peak of 33.0 ppbv/h. When VOCs are reduced by 20% without  
417 accounting for the reductions in  $\alpha$ , the turning point for  $NO_x$  decreases to 1.26 ppbv with the  $P(O_3)$   
418 peak decreasing to 30.1 ppbv/h. When the reduction of  $\alpha$  is considered alongside the decrease in VOCs  
419 ( $\alpha$  decreases to 0.0265), the peak of  $P(O_3)$  remains the same as the initial case. Consequently,  
420 neglecting the  $\alpha$  changes is likely to overestimate the effectiveness of emission control. Our  
421 observations indicated that  $NO_x$  in Shanghai was notably high, which accords with the conditions to  
422 the right of the turning point in Fig. 9a. In this case, the major chain-termination reaction of the  $HO_x$   
423 cycle is the reaction between OH and  $NO_2$  to produce  $HNO_3$ , while the share of the reaction that  
424 produces ANs through the reaction between  $RO_2$  and NO becomes relatively minor. As illustrated in  
425 Fig. 9a, when  $NO_x$  changes from 22.0 to 1.0 ppbv, the impact of  $\alpha$  change will be larger, as the  $P(O_3)$   
426 difference between the two cases ranges from 0.1 to 2.6 ppbv/h. Therefore, the variation of  $\alpha$  has a  
427 limited impact on  $O_3$  production at high  $NO_x$ , whereas it offsets the impact of VOCs reduction as  $NO_x$   
428 decrease to around 1.5 ppbv which represents a low- $NO_x$  emission condition. In addition, the  
429 sensitivity analyses in a reduced VOC condition show that neglecting the  $\alpha$  change still overestimates  
430 the impact of VOCs reduction on  $P(O_3)$  by around 4 times with  $NO_x$  of 1 ppbv (Fig. 9b), which is also  
431 more significant than the case in Shanghai campaign. Therefore, the variation in  $\alpha$  has a temporarily  
432 limited impact on  $O_3$  production, whereas it should be seriously considered as  $NO_x$  levels continue to

433 decrease.



434

435 **Figure 9.** The ozone production rate ( $P(O_3)$ ) varies as a function of  $NO_x$  under different VOC- $NO_x$  regimes  
 436 during Shanghai campaign: (a) under mean measured parameters during the whole campaign (solid line, VOC  
 437 reactivity ( $K_{OH}$ ) of  $4.3/s$ , ANs branching ratio ( $\alpha$ ) of  $0.053$ ); a  $20\%$  reduction in  $K_{OH}$  with a  $50\%$  reduction in  $\alpha$   
 438 (red dot line,  $3.4/s$ ,  $0.0265$ ); a  $20\%$  reduction in  $K_{OH}$  with no change in  $\alpha$  (blue dot line,  $3.4/s$ ,  $0.053$ ). (b) under  
 439 observed parameters during the clean days (solid line,  $K_{OH}$  of  $2.0/s$ ,  $\alpha$  of  $0.053$ ); a  $20\%$  reduction in  $K_{OH}$  with a  
 440  $50\%$  reduction in  $\alpha$  (red dot line,  $1.6/s$ ,  $0.0265$ ); a  $20\%$  reduction in  $K_{OH}$  with no change in  $\alpha$  (blue dot line,  $1.6/s$ ,  
 441  $0.053$ ). Dash lines show the turning point in different cases.

442 To further investigate the effect of ANs formation on  $O_3$  production during different days,  
 443 sensitivity tests on VOCs reactivity and  $\alpha$  are conducted based on typical conditions during different  
 444 periods. The  $\alpha$  values are derived as  $0.055$ ,  $0.054$  and  $0.052$ , for the high ozone, clean and background  
 445 periods, respectively. As shown in Fig. S4, the  $P(O_3)$  exhibits a similar trend with the increase of  $NO_x$   
 446 across different periods. The  $P(O_3)$  peak during the background period ( $30.3$  ppbv/h) is slightly lower  
 447 than that during both the high ozone days and the clean days ( $32.5$  and  $32.4$  ppbv/h). Therefore, the  
 448 ANs chemistry has similar effects on  $O_3$  production within different periods during the Shanghai  
 449 campaign. Further comparisons of ozone production under varying precursor levels were conducted  
 450 using historical observations collected in August 1994 at Mecklenburg-Vorpommern Mankmoos (MK),  
 451 Germany (Ehhalt, 1999), and during the spring of 2006 in Mexico City (MX) (Farmer et al., 2011;  
 452 Perring et al., 2010). The MK site serves as a typical clean background location with a very low  
 453 effective  $\alpha$  of  $0.005$ , corresponding to  $\tau_{VOC}$  of  $0.4\text{ s}^{-1}$ , where methane is the predominant pollutant.  
 454 Conversely, the MX site is characterized as an urban environment with an effective  $\alpha$  of  $0.036$ , where  
 455 a total of  $58$  VOCs was measured, corresponding to  $\tau_{VOC}$  of  $3.1\text{ s}^{-1}$ . The MK site shows a peak of  
 456  $P(O_3)$  is  $2.2$  ppbv/h at the  $NO_x$  of  $0.63$  ppbv. In contrast, the MX site demonstrates a peak  $P(O_3)$  of  $7.2$   
 457 ppbv/h at a  $NO_x$  of  $1.9$  ppbv. Given that the Xinjin and Shanghai sites exhibit higher VOCs reactivity

458 than MX, the corresponding peak  $P(O_3)$  and the  $NO_x$  inflection point are significantly elevated. This  
459 increase is primarily attributed to the high  $P(HO_x)$ , coupled with a low  $\alpha$ , which substantially enhances  
460  $P(O_3)$  under the intensified  $HO_x$  cycling. Consequently, the ozone production potentials of urban sites  
461 in China are overall higher than in other regions, while the influence of  $\alpha$  appears to be weak.

462 **4. Conclusions**

463 This study reveals the abundances of PNs and ANs and quantifies their respective impacts on  $O_3$   
464 pollution based on the field campaign in Shanghai. They both showed higher values but less  
465 pronounced diurnal variation during the  $O_3$  pollution period than the clean period. The mechanism  
466 validation indicates that Berkeley mechanism generally outperforms in the simulation of organic  
467 nitrates. The ratio of PNs/ $O_3$  serves as a significant indicator of photochemistry. In comparison to the  
468 previous Xinjin campaign, the inhibition effect of PNs chemistry on daytime  $O_3$  production diminished,  
469 likely attributed to the lower production of PNs. For ANs, the model simulation demonstrated that the  
470 branching ratio ( $\alpha$ ) influences the  $NO_x$ -VOCs- $O_3$  sensitivity. The consideration of  $\alpha$  value not only  
471 alters the  $P(O_3)$  peak in EKMA but also resulted in low effectiveness of precursor reductions, as the  $\alpha$   
472 would change with the reduction of VOCs. It is worth mentioning that the complex polluted regions  
473 are usually characterized by high  $NO_x$  and  $HO_x$ . In that case, the contribution of chain-termination  
474 reactions that produce ANs could be reduced, leading to limited impact of AN chemistry on  $O_3$   
475 formation. The effect of ANs chemistry on  $O_3$  pollution control is therefore expected to enhance with  
476 further precursor reductions, and we suggest a pressing need for more measurements and analysis of  
477 organic nitrates to address the forthcoming challenges in air pollution mitigation.

478  
479 **Code/Data availability.** The datasets used in this study are available from the corresponding author  
480 upon request ([chenxr95@mail.sysu.edu.cn](mailto:chenxr95@mail.sysu.edu.cn); [k.lu@pku.edu.cn](mailto:k.lu@pku.edu.cn)).

481  
482 **Author contributions.** K.D.L. and X.R.C. designed the study. C.M.L. and X.R.C. analyzed the data  
483 and wrote the paper with input from K.D.L.

484  
485 **Competing interests.** The authors declare that they have no conflicts of interest.

486  
487 **Acknowledgments.** This work was supported by the National Natural Science Foundation of China  
488 (Grants No. 42407139); the National Natural Science Foundation of China (Grants No. 22406204);  
489 the special fund of State Environmental Protection Key Laboratory of Formation and Prevention of  
490 Urban Air Pollution Complex (SEPAir-2024080219); the Innovative Exploration Program of National  
491 Institute of Metrology, China (No. AKYCX2313).

## References

Arey J, Aschmann SM, Kwok ESC, Atkinson R. Alkyl Nitrate, Hydroxyalkyl Nitrate, and Hydroxycarbonyl Formation from the NO<sub>x</sub> – Air Photooxidations of C5 – C8 n-Alkanes. *The Journal of Physical Chemistry A* 2001; 105: 1020-1027.

Aruffo E, Di Carlo P, Dari-Salisburgo C, Biancofiore F, Giammaria F, Busilacchio M, et al. Aircraft observations of the lower troposphere above a megacity: Alkyl nitrate and ozone chemistry. *Atmospheric Environment* 2014; 94: 479-488.

Ashmore MR. Assessing the future global impacts of ozone on vegetation. *Plant Cell and Environment* 2005; 28: 949-964.

Browne EC, Cohen RC, Wooldridge PJ, Valin LC, Min K-E. Organic nitrate formation: Impacts on NO<sub>x</sub> lifetime and ozone. *Abstracts of Papers of the American Chemical Society* 2012; 244.

Browne EC, Min KE, Wooldridge PJ, Apel E, Blake DR, Brune WH, et al. Observations of total RONO<sub>2</sub> over the boreal forest: NO<sub>x</sub> sinks and HNO<sub>3</sub> sources. *Atmospheric Chemistry and Physics* 2013; 13: 4543-4562.

Chen J, Wu H, Liu AW, Hu SM, Zhang J. Field Measurement of NO<sub>2</sub> and RNO<sub>2</sub> by Two-Channel Thermal Dissociation Cavity Ring Down Spectrometer. *Chinese Journal of Chemical Physics* 2017; 30: 493-498.

Darer AI, Cole-Filipliak NC, O'Connor AE, Elrod MJ. Formation and Stability of Atmospherically Relevant Isoprene-Derived Organosulfates and Organonitrates. *Environmental Science & Technology* 2011; 45: 1895-1902.

Day DA, Dillon MB, Wooldridge PJ, Thornton JA, Rosen RS, Wood EC, et al. On alkyl nitrates, O-3, and the "missing NO<sub>y</sub>". *Journal of Geophysical Research-Atmospheres* 2003; 108.

Ehhalt DH. Photooxidation of trace gases in the troposphere. *Physical Chemistry Chemical Physics* 1999; 1: 5401-5408.

Farmer DK, Perring AE, Wooldridge PJ, Blake DR, Baker A, Meinardi S, et al. Impact of organic nitrates on urban ozone production. *Atmospheric Chemistry and Physics* 2011; 11: 4085-4094.

Fisher JA, Jacob DJ, Travis KR, Kim PS, Marais EA, Miller CC, et al. Organic nitrate chemistry and its implications for nitrogen budgets in an isoprene- and monoterpene-rich atmosphere: constraints from aircraft (SEAC(4)RS) and ground-based (SOAS) observations in the Southeast US. *Atmospheric Chemistry and Physics* 2016; 16: 5969-5991.

Flocke F, Volz-Thomas A, Buers HJ, Patz W, Garthe HJ, Kley D. Long-term measurements of alkyl nitrates in southern Germany 1. General behavior and seasonal and diurnal variation. *Journal of Geophysical Research-Atmospheres* 1998; 103: 5729-5746.

Gao W, Tie X, Xu J, Huang R, Mao X, Zhou G, et al. Long-term trend of O-3 in a mega City (Shanghai), China: Characteristics, causes, and interactions with precursors. *Science of the Total Environment* 2017; 603: 425-433.

Grosjean E, Grosjean D, Woodhouse LF, Yang YJ. Peroxyacetyl nitrate and peroxypropionyl nitrate in Porto Alegre, Brazil. *Atmospheric Environment* 2002; 36: 2405-2419.

Ito A, Sillman S, Penner JE. Global chemical transport model study of ozone response to changes in chemical kinetics and biogenic volatile organic compounds emissions due to increasing temperatures: Sensitivities to isoprene nitrate chemistry and grid resolution. *Journal of Geophysical Research-Atmospheres* 2009; 114.

Lee G, Jang Y, Lee H, Han J-S, Kim K-R, Lee M. Characteristic behavior of peroxyacetyl nitrate (PAN) in Seoul megacity, Korea. *Chemosphere* 2008; 73: 619-628.

Li C, Wang H, Chen X, Zhai T, Chen S, Li X, et al. Thermal dissociation cavity-enhanced absorption spectrometer for measuring NO<sub>2</sub>, RO<sub>2</sub>NO<sub>2</sub>, and RONO<sub>2</sub> in the atmosphere. *Atmospheric Measurement Techniques* 2021; 14: 4033-4051.

Li C, Wang H, Chen X, Zhai T, Ma X, Yang X, et al. Observation and modeling of organic nitrates on a suburban site in southwest China. *Science of the Total Environment* 2023; 859.

Liebmann J, Karu E, Sobanski N, Schuladen J, Ehn M, Schallhart S, et al. Direct measurement of NO<sub>3</sub> radical reactivity in a boreal forest. *Atmospheric Chemistry and Physics* 2018; 18: 3799-3815.

Liebmann J, Sobanski N, Schuladen J, Karu E, Hellen H, Hakola H, et al. Alkyl nitrates in the boreal forest: formation via the NO<sub>3</sub>-, OH- and O-3-induced oxidation of biogenic volatile organic compounds and ambient lifetimes. *Atmospheric Chemistry and Physics* 2019; 19: 10391-10403.

Ling ZH, Guo H, Simpson IJ, Saunders SM, Lam SHM, Lyu XP, et al. New insight into the spatiotemporal variability and source apportionments of C-1-C-4 alkyl nitrates in Hong Kong. *Atmospheric Chemistry and Physics* 2016; 16: 8141-8156.

Liu Y, Shen H, Mu J, Li H, Chen T, Yang J, et al. Formation of peroxyacetyl nitrate (PAN) and its impact on ozone production in the coastal atmosphere of Qingdao, North China. *Science of the Total Environment* 2021; 778.

Lu KD, Hofzumahaus A, Holland F, Bohn B, Brauers T, Fuchs H, et al. Missing OH source in a suburban environment near Beijing: observed and modelled OH and HO<sub>2</sub> concentrations in summer 2006. *Atmospheric Chemistry and Physics* 2013; 13: 1057-1080.

Monks PS, Archibald AT, Colette A, Cooper O, Coyle M, Derwent R, et al. Tropospheric ozone and its precursors from the urban to the global scale from air quality to short-lived climate forcer. *Atmos. Chem. Phys.* 2015; 15: 8889-8973.

Ng NL, Brown SS, Archibald AT, Atlas E, Cohen RC, Crowley JN, et al. Nitrate radicals and biogenic volatile organic

550 compounds: oxidation, mechanisms, and organic aerosol. *Atmospheric Chemistry and Physics* 2017; 17: 2103-2162.  
551 Perring AE, Bertram TH, Farmer DK, Wooldridge PJ, Dibb J, Blake NJ, et al. The production and persistence of Sigma  
552 RONO<sub>2</sub> in the Mexico City plume. *Atmospheric Chemistry and Physics* 2010; 10: 7215-7229.  
553 Perring AE, Pusede SE, Cohen RC. An Observational Perspective on the Atmospheric Impacts of Alkyl and Multifunctional  
554 Nitrates on Ozone and Secondary Organic Aerosol. *Chemical Reviews* 2013; 113: 5848-5870.  
555 Perring AE, Wisthaler A, Graus M, Wooldridge PJ, Lockwood AL, Mielke LH, et al. A product study of the isoprene+NO<sub>3</sub>  
556 reaction. *Atmospheric Chemistry and Physics* 2009; 9: 4945-4956.  
557 Present PSR, Zare A, Cohen RC. The changing role of organic nitrates in the removal and transport of NO<sub>x</sub>. *Atmospheric  
558 Chemistry and Physics* 2020; 20: 267-279.  
559 Reisen F, Aschmann SM, Atkinson R, Arey J. 1,4-hydroxycarbonyl products of the OH radical initiated reactions of C-5-  
560 C-8 n-alkanes in the presence of NO. *Environmental Science & Technology* 2005; 39: 4447-4453.  
561 Roberts JM, Bertman SB. The thermal-decomposition of peroxyacetic nitric anhydride (pan) and peroxymethacrylic nitric  
562 anhydride (MPAN). *International Journal of Chemical Kinetics* 1992; 24: 297-307.  
563 Romer PS, Duffey KC, Wooldridge PJ, Allen HM, Ayres BR, Brown SS, et al. The lifetime of nitrogen oxides in an  
564 isoprene-dominated forest. *Atmospheric Chemistry and Physics* 2016; 16: 7623-7637.  
565 Romer PS, Duffey KC, Wooldridge PJ, Edgerton E, Baumann K, Feiner PA, et al. Effects of temperature-dependent NO<sub>x</sub>  
566 emissions on continental ozone production. *Atmospheric Chemistry and Physics* 2018; 18: 2601-2614.  
567 Rosen RS, Wood EC, Wooldridge PJ, Thornton JA, Day DA, Kuster W, et al. Observations of total alkyl nitrates during  
568 Texas Air Quality Study 2000: Implications for O<sub>3</sub> and alkyl nitrate photochemistry. *Journal of Geophysical  
569 Research-Atmospheres* 2004a; 109: 15.  
570 Rosen RS, Wood EC, Wooldridge PJ, Thornton JA, Day DA, Kuster W, et al. Observations of total alkyl nitrates during  
571 Texas Air Quality Study 2000: Implications for O<sub>3</sub> and alkyl nitrate photochemistry. *Journal of Geophysical  
572 Research-Atmospheres* 2004b; 109.  
573 Sadanaga Y, Takaji R, Ishiyama A, Nakajima K, Matsuki A, Bandow H. Thermal dissociation cavity attenuated phase shift  
574 spectroscopy for continuous measurement of total peroxy and organic nitrates in the clean atmosphere. *Review of  
575 Scientific Instruments* 2016; 87.  
576 Schwantes RH, Emmons LK, Orlando JJ, Barth MC, Tyndall GS, Hall SR, et al. Comprehensive isoprene and terpene gas-  
577 phase chemistry improves simulated surface ozone in the southeastern US. *Atmospheric Chemistry and Physics* 2020;  
578 20: 3739-3776.  
579 Shepson PB, Hastie DR, So KW, Schiff HI. Relationships between PAN, PPN and O<sub>3</sub> at urban and rural sites in Ontario.  
580 *Atmospheric Environment Part a-General Topics* 1992; 26: 1259-1270.  
581 Song J, Zhang Y, Huang Y, Ho KF, Yuan Z, Ling Z, et al. Seasonal variations of C-1-C-4 alkyl nitrates at a coastal site in  
582 Hong Kong: Influence of photochemical formation and oceanic emissions. *Chemosphere* 2018; 194: 275-284.  
583 Sun J, Li Z, Xue L, Wang T, Wang X, Gao J, et al. Summertime C-1-C-5 alkyl nitrates over Beijing, northern China: Spatial  
584 distribution, regional transport, and formation mechanisms. *Atmospheric Research* 2018; 204: 102-109.  
585 Sun M, Cui Jn, Zhao X, Zhang J. Impacts of precursors on peroxyacetyl nitrate (PAN) and relative formation of PAN to  
586 ozone in a southwestern megacity of China. *Atmospheric Environment* 2020; 231.  
587 Tan Z, Fuchs H, Lu K, Hofzumahaus A, Bohn B, Broch S, et al. Radical chemistry at a rural site (Wangdu) in the North  
588 China Plain: observation and model calculations of OH, HO<sub>2</sub> and RO<sub>2</sub> radicals. *Atmos. Chem. Phys.* 2017a; 17: 663-  
589 690.  
590 Tan Z, Fuchs H, Lu K, Hofzumahaus A, Bohn B, Broch S, et al. Radical chemistry at a rural site (Wangdu) in the North  
591 China Plain: observation and model calculations of OH, HO<sub>2</sub> and RO<sub>2</sub> radicals. *Atmospheric Chemistry and Physics* 2017b; 17: 663-690.  
592 Tan Z, Lu K, Jiang M, Su R, Dong H, Zeng L, et al. Exploring ozone pollution in Chengdu, southwestern China: A case  
593 study from radical chemistry to O<sub>3</sub>-VOC-NO<sub>x</sub> sensitivity. *Sci Total Environ* 2018a; 636: 775-786.  
594 Tan ZF, Rohrer F, Lu KD, Ma XF, Bohn B, Broch S, et al. Wintertime photochemistry in Beijing: observations of RO<sub>x</sub>  
595 radical concentrations in the North China Plain during the BEST-ONE campaign. *Atmospheric Chemistry and Physics*  
596 2018b; 18: 12391-12411.  
597 Teng AP, Crounse JD, Lee L, St Clair JM, Cohen RC, Wennberg PO. Hydroxy nitrate production in the OH-initiated  
598 oxidation of alkenes. *Atmospheric Chemistry and Physics* 2015; 15: 4297-4316.  
599 Travis KR, Jacob DJ, Fisher JA, Kim PS, Marais EA, Zhu L, et al. Why do models overestimate surface ozone in the  
600 Southeast United States? *Atmospheric Chemistry and Physics* 2016; 16: 13561-13577.  
601 Wang M, Shao M, Chen W, Lu S, Wang C, Huang D, et al. Measurements of C1-C4 alkyl nitrates and their relationships  
602 with carbonyl compounds and O<sub>3</sub> in Chinese cities. *Atmospheric Environment* 2013; 81: 389-398.  
603 Wang W, Parrish DD, Wang S, Bao F, Ni R, Li X, et al. Long-term trend of ozone pollution in China during 2014-2020:  
604 distinct seasonal and spatial characteristics and ozone sensitivity. *Atmospheric Chemistry and Physics* 2022; 22: 8935-  
605 8949.

607 Xu T, Nie W, Xu Z, Yan C, Liu Y, Zha Q, et al. Investigation on the budget of peroxyacetyl nitrate (PAN) in the Yangtze  
608 River Delta: Unravelling local photochemistry and regional impact. *Science of the Total Environment* 2024; 917.

609 Xue K, Zhang X. The rationale behind updates to ambient ozone guidelines and standards. *Frontiers in Public Health* 2023;  
610 11.

611 Yeh GK, Ziemann PJ. Alkyl Nitrate Formation from the Reactions of C<sub>8</sub>-C<sub>14</sub>-n-Alkanes  
612 with OH Radicals in the Presence of NO<sub>x</sub>: Measured Yields with Essential Corrections for Gas-  
613 Wall Partitioning. *Journal of Physical Chemistry A* 2014a; 118: 8147-8157.

614 Yeh GK, Ziemann PJ. Identification and Yields of 1,4-Hydroxynitrates Formed from the Reactions of C<sub>8</sub>-  
615 C<sub>16</sub>-n-Alkanes with OH Radicals in the Presence of NO<sub>x</sub>. *Journal of Physical Chemistry A* 2014b; 118: 8797-8806.

616 Young PJ, Naik V, Fiore AM, Gaudel A, Guo J, Lin MY, et al. Tropospheric Ozone Assessment Report: Assessment of  
617 global-scale model performance for global and regional ozone distributions, variability, and trends. *Elementa -Science  
618 of the Anthropocene* 2018; 6.

619 Zare A, Romer PS, Tran N, Keutsch FN, Skog K, Cohen RC. A comprehensive organic nitrate chemistry: insights into the  
620 lifetime of atmospheric organic nitrates. *Atmospheric Chemistry and Physics* 2018; 18: 15419-15436.

621 Zeng L, Fan G-J, Lyu X, Guo H, Wang J-L, Yao D. Atmospheric fate of peroxyacetyl nitrate in suburban Hong Kong and  
622 its impact on local ozone pollution. *Environmental Pollution* 2019; 252: 1910-1919.

623 Zhang B, Zhao X, Zhang J. Characteristics of peroxyacetyl nitrate pollution during a 2015 winter haze episode in Beijing.  
624 *Environmental Pollution* 2019; 244: 379-387.

625 Zhang G, Xia L, Zang K, Xu W, Zhang F, Liang L, et al. The abundance and inter-relationship of atmospheric peroxyacetyl  
626 nitrate (PAN), peroxypropionyl nitrate (PPN), O<sub>3</sub>, and NO<sub>y</sub> during the wintertime in Beijing, China. *Science of the  
627 Total Environment* 2020; 718.

628 Zhang H, Tong S, Zhang W, Xu Y, Zhai M, Guo Y, et al. A comprehensive observation on the pollution characteristics of  
629 peroxyacetyl nitrate (PAN) in Beijing, China. *Science of the Total Environment* 2023; 905.

630 Zhang H, Xu X, Lin W, Wang Y. Wintertime peroxyacetyl nitrate (PAN) in the megacity Beijing: Role of photochemical  
631 and meteorological processes. *Journal of Environmental Sciences* 2014; 26: 83-96.

632 Zhang JM, Wang T, Ding AJ, Zhou XH, Xue LK, Poon CN, et al. Continuous measurement of peroxyacetyl nitrate (PAN)  
633 in suburban and remote areas of western China. *Atmospheric Environment* 2009; 43: 228-237.

634 Zhu W, Zhou M, Cheng Z, Yan N, Huang C, Qiao L, et al. Seasonal variation of aerosol compositions in Shanghai, China:  
635 Insights from particle aerosol mass spectrometer observations. *Science of The Total Environment* 2021; 771: 144948.

636

637